Transactions, SMiRT-26
Berlin/Potsdam, Germany, July 10-15, 2022
Division VII

FAILURE MECHANISM AND FRAGILITY ANALYSIS OF RC BOX CULVERT SUBJECTED TO FAULT RUPTURE DISPLACEMENT

Tomohiro Sasaki[1], Shunichi Higuchi[2]

[1] Research Engineer, Obayashi Corp., Japan (sasaki.tomohiro@obayashi.co.jp)
[2] General Manager, Obayashi Corp. Japan

ABSTRACT

Underground structures may suffer significant damage subjected to the fault rupture. This research investigates the failure mechanisms of a RC box culvert subjected to fault displacement based on a 2D FE analysis and a fragility analysis was performed in terms of variation on concrete and soil strength, as well as soil stiffness. Based on the analytical results, it is found for a low-angle fault that the failure probability of the RC box culvert is significantly affected by the soil stiffness variation, rather than by the strength variation of materials. On the other hand, the failure probability of the RC box culvert for a high-angle fault is affected not only by the soil stiffness variation but also by the material strength variation.

INTRODUCTION

Underground structure may suffer significant damage subjected to the fault rupture (Earthquake Engineering Committee, JSCE 2011). In the 2016 Kumamoto earthquake, large ground deformations were confirmed on the ground surface due to fault displacement exceeding 2 m (Yoshimi 2017), and it was pointed out that the structures may have been damaged by these ground deformations (Chida 2017).

Generally, underground structures have high seismic resistance capability. However, once a fault crossing the underground structure occurs, it suffers significant damage due to large ground deformation. Recently, research on such a fault displacement has been performed. Higuchi et al. (2017) conducted centrifuge experiment and finite element analysis of box culvert subjected to fault displacement and found that the earth pressure acting at the top slab keeps initial earth pressure while that acting at the side walls increases and deformation and earth pressure can be represented by finite element (FE) analysis with the subloading surface model proposed by Hashiguchi (2017).

In this research, the fragility analysis based on a series of 2D FE analyses using the same model validated by Higuchi (2017) was performed in terms of variation on concrete and soil strength as well as soil stiffness to clarify relationship between material parameters and failure mechanism.

FE ANALYSIS MODEL AND FRAGILITY EVALUATION

Figure 1 shows target structure, which is same model as the past research (Sasaki and Higuchi 2018). It is 9.5 m wide, 5.5 m tall RC box culvert with two inner spaces and designed based on Design Standards for Railway Structures in Japan (RTRI 1999). Overburden of 20 m, dry dense sandy soil with a density of 17 kN/m^3, and the coefficient of earth pressure of 0.5 are assumed respectively, for soil around the structure. The bedrock is modelled as the lower boundary. Therefore, bedrock is rigid.

Figure 2 shows numerical model for 2D FE analysis in this research. Two-dimensional quadrilateral plane strain elements are applied to RC Box Culvert and soil. The smeared crack model with embedded reinforcements (Naganuma et al. 2004) and the subloading surface model (Hashiguchi 2017) are used as the hysteresis model of RC and soil, respectively. The parameters for the subloading surface model are shown in Table 1. These parameters obtained from centrifuge experiments conducted by Higuchi (2017) and they are capable of adequately reproducing the soil pressure acting on the underground structure subjected to the fault displacement. These parameters can reproduce the consolidated-drained triaxial test, and the analysis using these parameters adequately reproduced the experimental results of soil pressure acting on each face of the structure, as well as the deformation mode of the structure and the ground surface displacement.

Joint elements are used between soil and structure, between soil and bedrock, between structure and bedrock to account for contact and separation. In the normal direction of the elements, the contact model is used in which force transfer occurs with high stiffness in the direction of contact of the joint elements and zero force as the elements are separated. In the shear direction, the friction model with a friction angle of 35 degrees is used.

In this analysis, it is assumed that a reverse fault occurred below the RC box culvert in the transverse direction of the culvert axis. The fault line is assumed to be located at 2.5 m from the right edge of the structure (about 1/4 of the total width), and the bedrock moves up from lower right to upper left. As for the fault angle, two cases are studied; 30 and 60 degrees (in Figure 2 the first case is shown). Fault displacement was simulated by applying forced displacement to the node on the right side (upper side) while restraining the displacement of the node on the left side (lower side) of the fault. Fault displacements were applied in increments of 0.02 mm per analysis step, with a maximum fault displacement of 400 mm (20,000 steps).

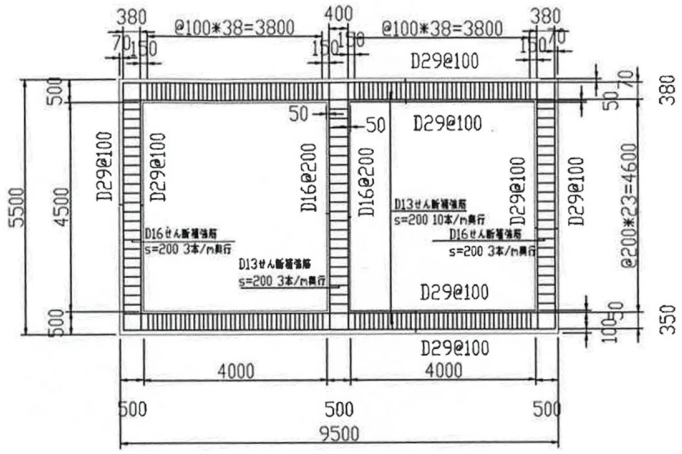

Figure 1 Target Structure

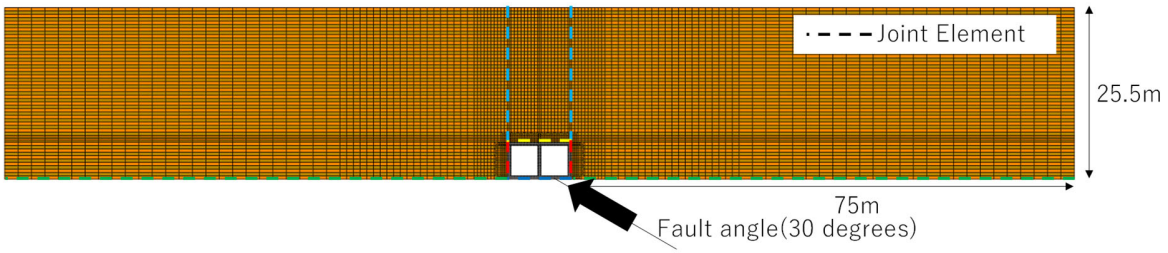

Figure 2. Numerical Model for FE Analysis

Table 1 Parameters for Subloading Surface Model

Item		Value
Compression Index	λ	0.0074
Swelling Index	κ	0.0039
Initial Void Ratio	e_0	0.73
Internal Friction Angle	ϕ	32 deg
Poisson's Ratio	ν	0.33
OCR	P_c/σ'_m	10
Rotational Hardening		Not Considered
Shear Hardening/Softening Coefficient	μ	0.25
Evolution of Normal Yield Ratio	u	100
Reference Average Stress	σ'_{mref}	100 kN/m^2

In the fragility analysis, aleatory uncertainty is modelled for three material parameters: concrete compressive strength, shear wave velocity corresponding to ground stiffness, and internal friction angle corresponding to ground strength. Table 2 shows the variation of the three material parameters. The realistic response is obtained based on the analysis of $2^3 = 8$ cases (combinations of $\mu + \sigma$ and $\mu - \sigma$ for each material parameters) considering the variations shown in Table 2, and the realistic capacity calculated considering the aleatory uncertainties in the compressive strength of concrete was evaluated. The limit states of the structure are determined for each of those cases and the corresponding fragility parameters were evaluated using two-point estimation method (Rosenblueth 1981). The limit states of the members are defined based on the rebar strain. The flexural yield is defined as the main rebar yielding and the diagonal shear failure is defined as the shear reinforcement yielding.

The fragility curve is defined as the conditional probability $F(\alpha)$ that the ratio of the strain of each rebar, the realistic response, to the yield strain of each rebar, the realistic capacity, exceeds 1 at a given fault displacement α. The coefficient of variation (CV) for each parameter is set based on AESJ (2007). It is noted that the compressive strength of the concrete is assumed to vary with the tensile strength of the concrete, while Young's modulus is assumed to remain unchanged (AESJ 2007). The probability density functions for the realistic response and realistic capacity are assumed to be a log-normal distribution, and the log standard deviation for the epistemic uncertainty is assumed to be 0.15 (AESJ 2007).

Table 2 Variation of Material Parameters for Fragility Analysis

	Average μ	$\mu + \sigma$	$\mu - \sigma$	CV
Concrete Compressive Strength	1.4 × Design strength 33.6 MPa	1.13μ 38.0 MPa	0.87μ 29.6 MPa	$CV = 0.13$
Soil Stiffness	Shear wave velopcity $V_s = 200$ m/s	1.1μ $V_s = 220$ m/s	0.9μ $V_s = 180$ m/s	$CV = 0.1$
Soil Strength	Internal Friction Angle in Table 1 $\phi = 32$ deg	1.1μ $\phi = 34.5$ deg	0.9μ $\phi = 29.4$ deg	$CV = 0.1$ for $\tan\phi$

EFFECT OF FAULT ANGLE ON FAILURE MECHANISM

Firstly, analyses focusing on the effect of different fault angles on the damage mechanism of RC box culverts using the average material parameters shown in Table 2, were conducted.

Figure 3 shows the maximum shear strain distribution of the soil at a fault displacement of 400 mm. At a low fault angle of 30 degrees, there is a region of large maximum shear strain located mainly on the left wall, and a region of large maximum shear strain extends horizontally, forming the active wedge by the soil movement. Nearly 10 % maximum shear strain occurred in the ground around the upper left corner of the structure.

On the other hand, at the high fault angle of 60 degrees, a region of large maximum shear strain extends directly above the top slab and the ground surface above the structure is deformed. Because of the high fault angle of 60 degrees, the vertical component of fault displacement is larger than the horizontal component, indicating that the fault deformation was caused by thrusting from below. The upper left corner of the structure had a maximum shear strain of nearly 10 %, almost the same as the 30-degree fault angle. A large maximum shear strain of about 2 % was also observed at a location on the ground surface slightly displaced from directly above the structure to the upper plate (moving bedrock) side.

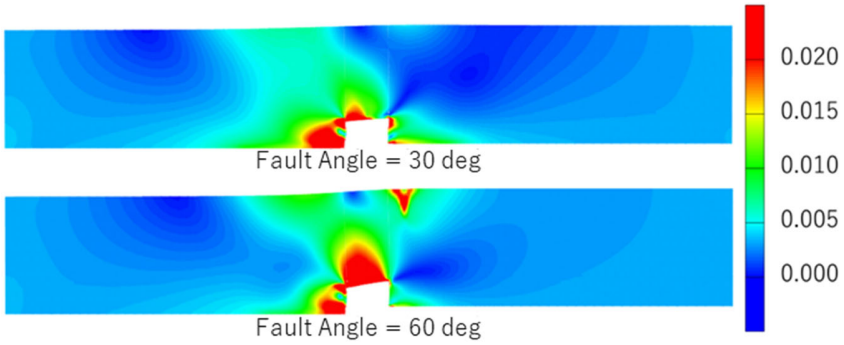

Figure 3 Maximum Shear Strain at the Fault Displacement of 400 mm

Figure 4 shows the stress paths of the soil elements close to the middle height of the left wall. At a fault angle of 30 degrees, the stress state of the soil is below the critical state line (C.S.L.) and the ground does not yield up to a fault displacement of 400 mm. In contrast, at a fault angle of 60 degrees, the ground yields beyond the C.S.L. at a fault displacement of 261 mm. When the fault angle is 30 degrees, the horizontal displacement component is larger than vertical one, and the soil close to the left wall does not yield because the effective stress p increases due to increase of horizontal normal stress, and the soil strength

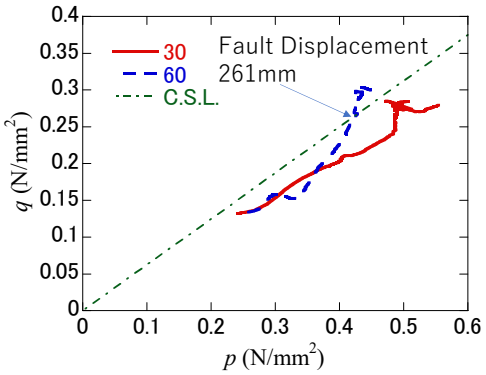

Figure 4 Stress Path of the Soil Element close to the Middle height of Left Wall

increases faster than the shear stress. On the other hand, when the fault angle is 60 degrees, the vertical component of fault displacement is larger than horizontal one, and the frictional force between the left wall and the soil causes large shear deformation in the soil and the ground yields.

Figure 5 shows the distribution of rebar strain at a fault displacement of 400 mm. The horizontal rebars correspond to the main bars in the top and bottom slabs, and to shear reinforcements in the walls. The vertical rebars correspond to shear reinforcements in the top and bottom slabs, and main bars in the walls. In addition, the white elements shown in Figure 5 means there are no rebars in that direction.

In both the 30- and 60-degree fault angle, the right wall is displaced upward due to the upward displacement of the moving bedrock, while the left wall is subjected to downward frictional forces from the ground on the left side of the structure, so that the structure is deformed like a cantilever beam with the fixed end at the right wall and free end at the left wall. As a result, tensile yielding occurs in the upper main bar at the right end of the top slab. Bending deformation also occurs at the upper and lower ends of the partition wall (center wall, hereafter) due to the deformation of the top and bottom plates. In particular, at a fault angle of 60 degrees, greater vertical displacement occurs, resulting in tensile yielding of the upper reinforcement at the top plate's junction with the middle wall.

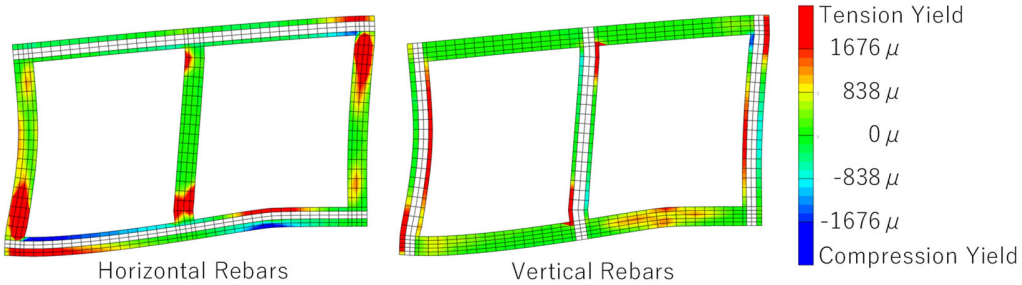

(a) Fault angle = 30 deg

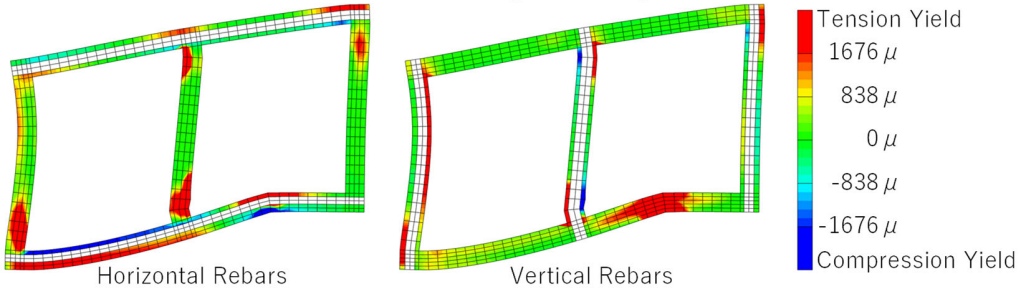

(b) Fault angle = 60 deg

Figure 5 Rebar Strain Distribution at the Fault Displacement of 400 mm

The shear force at the bottom of the left wall is shown in Figure 6. The shear force is evaluated by summation of the element shear forces (product of element shear stress with respective cross-sectional area). Figure 6 also shows the shear capacity considering distributed loads (Saito et al. 2004). The shear capacity considering distributed loads is a method of evaluating shear capacity by replacing distributed loads with multiple concentrated loads. It should be noted that this method is more accurate for evaluating shear capacity for distributed loads caused by earth pressure than evaluating shear capacity by an equivalent single concentrated load (Sasaki and Higuchi 2018).

As shown in Figure 6, the damage mechanism is almost same in both 30- and 60-degree fault angle. First flexure yield occurs in order of the center wall, bottom slab and right wall and finally shear

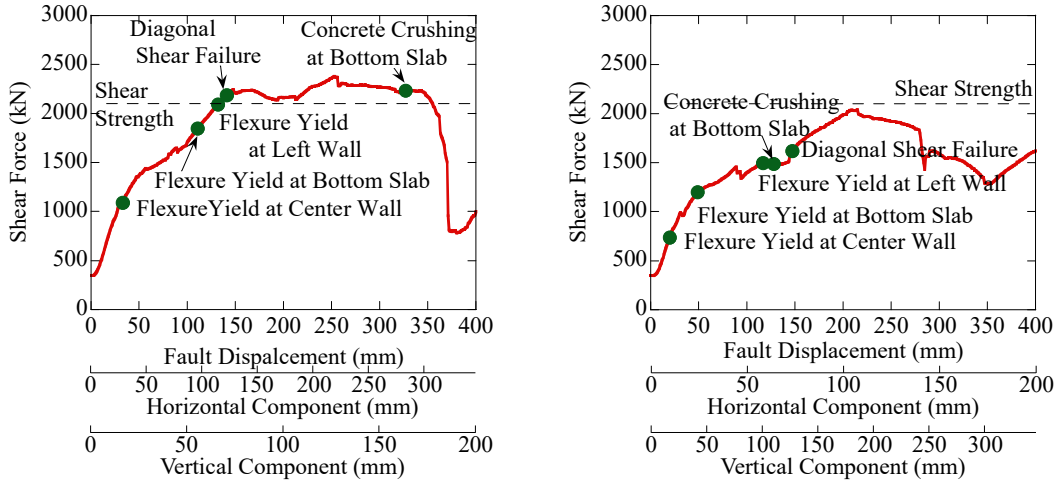

(a) Fault angle = 30 deg (b) Fault angle = 60 deg

Figure 6 Shear Force at the Bottom End of Left Wall

reinforcements at the left wall yield and failed in diagonal shear. Flexure yield at the center wall and bottom slab occurs when the vertical component of fault displacement reaches 16-17 mm in both 30- and 60-degree fault angle. However, as shown in Figure 5, the rebar strain in the center wall and bottom slab is larger the more severe damage occurs in these members at a fault angle of 60 degrees, than at a fault angle of 30 degrees. Note that the crushing of concrete at the compression edge in the bottom slab occurs at a fault displacement of 327 mm for a fault angle of 30 degrees, while that occurs at a smaller fault displacement of 127 mm for a fault angle of 60 degrees. This fact also indicates that the damage to the bottom slab is more severe for a fault angle of 60 degrees than that of 30 degrees.

The flexure yield of the left wall occurs when the fault displacement reached 132 mm at a low fault angle of 30 degrees and 117 mm at a high fault angle of 60 degrees. When the structure is thrust up by a reverse fault, frictional forces with the surrounding ground are applied downward and axial tensile forces are introduced into the left side wall. Therefore, it is considered that the higher fault angle resulted in earlier flexure yield. On the other hand, yielding of the shear reinforcements in the left wall occurs at approximately the same fault displacement of 141 to 146 mm, regardless of the fault angle. It is also noted that the maximum shear force acting at the bottom of the left wall and the shear capacity are close. This shows that the estimate of the shear capacity by distributed loads is quite accurate in this case.

FRAGILITY EVALUATION

Figure 7 shows the fragility curves calculated based on the analysis with varying soil stiffness, soil strength, and concrete strength. The points in Figure 7 represent the damage probabilities obtained based on the realistic responses obtained from the analysis, and the solid line shows the approximated cumulative lognormal distribution curves of the relationship between fault displacement and damage probability, which represents these points. Also shown in Figure 7 are the damage probabilities at the 5 % and 95 % confidence levels when epistemic uncertainty is considered with dashed and single-pointed lines, respectively.

For the limit state “yielding of the center wall,” the fault displacement capacity is about 26 mm (HCLPF value: fault displacement with less than 5 % probability of failure at 95 % confidence level) to 30 mm (50 % probability of failure: fault displacement with 50 % probability of failure at 50 % confidence level) for a fault angle of 30°, whereas for a fault angle of 60°, the fault displacement capacity is about 14 mm (HCLPF value) to 20 mm (50 % damage probability), and these vertical components are roughly equal. On the other hand, for the limit state “diagonal shear failure,” the fault displacement capacity is about 95

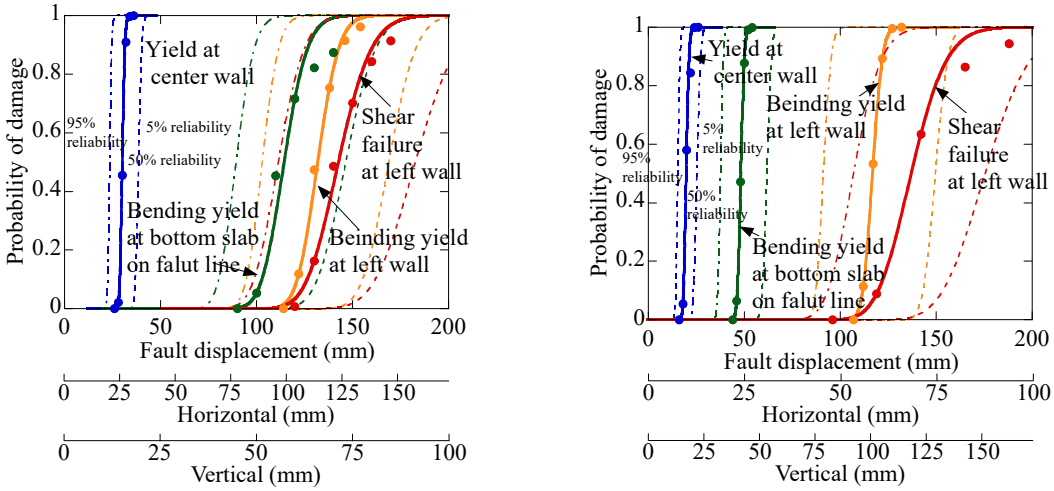

(a) Fault angle = 30 deg (b) Fault angle = 60 deg

Figure 7 Fragility Curves

Table 3 Log Standard Deviation of Aleatory Uncertainty Factors for Each Material Parameter

(a) Fault Angle of 30 Degrees

	Total	Concrete Strength β_c	Soil Stiffness β_G	Soil Strength β_ϕ
Flexural Yield of Center Wall	0.040	0.031 (37 %)	0.040 (62 %)	0.006 (14 %)
Diagonal Shear Failure of Left Wall	0.095	0.025 (7 %)	0.094 (91 %)	0.014 (2 %)

(b) Fault Angle of 60 Degrees

	Total	Concrete Strength β_c	Soil Stiffness β_G	Soil Strength β_ϕ
Flexural Yield of Center Wall	0.058	0.039 (41 %)	0.046 (57 %)	0.008 (2 %)
Diagonal Shear Failure of Left Wall	0.105	0.049 (23 %)	0.079 (59 %)	0.045 (19 %)

mm (HCLPF value) to 143 mm (50 % damage probability) for a fault angle of 30 degrees, and 90 mm (HCLPF value) to 137 mm (50 % damage probability) at a fault angle of 60 degrees. Thus, the fault displacement capacity for the limit state “diagonal shear failure” is similar for both fault angles (30 and 60 degrees).

To evaluate the extent to which the three material parameters considered in this study affect the variability of the results, the log standard deviation of the aleatory uncertainty factor is calculated for each material parameter as shown in Table 3. The log standard deviations of the aleatory uncertainty factors for each parameter shown here is defined in this study in terms of the realistic response for the respective parameters, while averaging over response variation injected by the other parameters. For example, the aleatory uncertainty for concrete strength is evaluated based on the following procedure; 1) the realistic response of the model with higher concrete strength is obtained by averaging the four realistic responses obtained from the analysis of the four models varying soil stiffness and strength, 2) the realistic response

of the model with lower concrete strength is obtained by averaging the remained four realistic response, 3) the log standard deviations of the aleatory uncertainty for the concrete strength is calculated using two realistic response evaluated in 1) and 2) based on two point estimation method (Rosenblueth 1981). The contribution of the variation of each material parameter, shown in parenthesis in Table 3, is evaluated with the following equation.

$$R_i = \frac{{\beta_i}^2}{{\beta_c}^2 + {\beta_G}^2 + {\beta_\phi}^2} \times 100\ (\%)\ (i = c, G, \phi) \tag{1}$$

Note that β_c, β_G, β_ϕ are the log standard deviation of the aleatory uncertainty factor for concrete strength, soil stiffness and soil strength, respectively, and R_c, R_G, R_ϕ are contribution for concrete strength, soil stiffness and soil strength, respectively.

As shown in Table 3, for the limit state "flexural yield of center wall" the contribution for concrete strength and soil stiffness is larger than that for soil strength when the flexural yield of center wall occurs in both the fault angle (30 and 60 degrees). On the other hand, for the limit state "diagonal shear failure" the contribution of soil stiffness is dominant value of 91% while the contribution of concrete and soil strength is negligible in the fault angle of 30 degrees. In contrast, for the fault angle of 60 degrees, the contribution of soil stiffness become smaller to 59% and the contribution of concrete and soil strength become larger to 19-23%, because the soil close to left wall yields as shown in Figures 3 and 4.

CONCLUSIONS

A two-dimensional finite element analysis is performed on a RC box culvert in a dense sand with overburden of 20 m, subjected to the displacements of a 30- and 60-degree reverse fault. Fragility curves based on the 2D FE analysis varying the concrete strength, soil stiffness and soil strength and the log standard deviation of the aleatory uncertainty factor for each material parameter are evaluated. The following conclusions are deduced;

1) The failure mechanism of the target RC box culvert used in this study is the same regardless of the fault angle; flexural yielding occurs in order of the center wall, bottom slab and left wall first, and finally shear reinforcements in the left wall yields and the left wall failed in diagonal shear.

2) Soil close to the left wall does not yield in the case "fault angle = 30 degrees." On the other hand, soil close to the left wall yields in the case "fault angle = 60 degrees" because the larger vertical component of fault displacement results in the friction force acting at the interface between the left wall and ground, and shear stress close to the left wall becomes larger by this friction force. The higher fault angle may lead larger soil damage.

3) Flexure yielding of the center wall occurs when the vertical component of fault displacement reaches 16 to 17 mm. The vertical component is dominant while the fault angle is not influential. On the other hand, the diagonal shear failure occurs at the fault displacement of 117-132mm, which is the same magnitude in both cases "fault angle = 30 and 60 degrees."

4) For the limit state "flexural yield of the center wall," the contribution of the log standard deviation of the aleatory uncertainty factor for concrete strength and soil stiffness is larger than that for soil strength in both cases "fault angles = 30 and 60 degrees."

5) For the limit state "diagonal shear failure," in the case "fault angle = 30 degrees," the contribution of the log standard deviation of the aleatory uncertainty factor for soil stiffness is dominant value of 91% while that for concrete and soil strength is negligible. In contrast, in the case "fault angle =

60 degrees," the contribution for soil stiffness become smaller to 59% and the contribution for concrete and soil strength become larger to 19-23%, because the soil close to left wall yields.

REFERENCES

Earthquake Engineering Committee, JSCE: *Seismic Performance Verification of Underground Structures and Earthquake Countermeasure Guidelines*, 2011 (in Japanese).

Yoshimi, M: "Fault activity and ground deformation," *1st Anniversary Damage Report Meeting of 2016 Kumamoto Earthquake*, Earthquake Engineering Committee, JSCE, http://committees.jsce.or.jp/eec2/system/files/06_20170422JSCE-yoshimi-2in1s_0.pdf, 2017 (in Japanese).

Chida, T., Watanabe, H., Taniguchi, R. and Choi, J.: "Study on Collapse Mechanism of Aso Bridge based on Static Analysis considering Sliding of Arch Abutment," *Proc. 20th Symposium of Seismic Design of Bridges*, JSCE, pp. 187-192, 2017 (in Japanese).

Higuchi, S., Kato, I., Sato, S., Itho, G. and Sato, Y.: "Experimental and Numerical Study on the Characteristics of Earth Pressure acting on the Box-Shape Underground Structure subjected the Strike Slip Fault Displacement," *J. JSCE*, Vol. 73, No. 4, pp. I_19-I_31, 2017 (in Japanese).

Hashiguchi, K.: *Foundations of Elastoplasticity: Subloading Surface Model*, Springer, 819 p., 2017.

RailwayTechnical Research Institute: *Design Standard for Railway Structures: Seismic Design*, Maruzen, 418 p., 1999.

Sasaki, T. and Higuchi, S.: "Failure Mechanism of Box Culvert subjected to Fault Rapture displacement," *J. JSCE*, Vol. 74, No. 4, pp. I_395-I_406, 2018 (in Japanese).

Naganuma, K., Yonezawa, K., Kurimoto, O. and Eto, H: "Simulation of Nonlinear Dynamic Response of Reinforced Concrete Scaled Model Using Three Dimensional Finite Element Method," *Proc. 13th WCEE*, Paper No.586, 2004.

Atomic Energy Society of Japan: *Standard of the Atomic Energy Society of Japan Criteria for Probabilistic Safety Assessment of Nuclear Power Plants Due to Earthquakes: 2007*, AESI-SC-P006:2007, 636 p., 2007.

Rosenblueth, E.: "Two-point Estimates in Probabilities," *Appl. Math. Modelling*, Vol. 5, pp. 329-335, 1981.

Saito, K., Takahashi, H., Ishibashi, T., Maruyama, K., Akiyama, M. and Suzuki, M.: "The Shear Strength of Reinforced Concrete Beams under Multiple Points Load," *J. JSCE*, Vol. 2004, No. 767/V-64, pp. 87-98, 2004 (in Japanse).